Benha Journal of Applied Sciences (BJAS) **print: ISSN 2356–9751**
Vol. (10) Issue (4) (2025), (9- 18) **online: ISSN 2356–976x**
http://bjas.bu.edu.eg
engineering sciences

Developments in Dye-Sensitized Solar Cells to Increase Efficiency

Menah Allah S.Abd El Ghany[1], Mina D.Asham[1], Walid M.Soliman[1], and Kamal A.Soliman[2]
[1] Basic Engineering Sciences Dept., Benha Faculty of Engineering, Benha University, Benha, Egypt
[2] Physical Chemistry Dept., Faculty of Science, Benha University, Benha, Egypt
E-mail: menallah.abdelghani@bhit.bu.edu.eg

Abstract

Due to their affordability and eco-friendliness, dye sensitized solar cells are becoming more widely used as a yet strongly evolving strain of solar cells. We have examined the performance of dye-sensitized solar cells in this research through SCAPS-1D simulation. This model consisted of five layers fluorine-doped tin oxide (FTO)/electron transport layer TiO_2 (ETL)/Rhamnus tinctoria dye is active layer/ liquid electrolyte is hole transport layer (HTL)/platinum (Pt) is the back contact. The effect of ETL, HTL, and active layer thicknesses, working temperature, the affinity of ETL, and the interface between TiO_2 and active layer on different parameters of the dye sensitized solar cell (DSSC) are studied. Experimental data was used to determine some of the study's input parameters. The density functional theory (DFT) computations were used to analyze the electronic characteristics. Each state's open circuit voltage (V_{OC}), short circuit current density (J_{SC}), fill factor (FF), and power conversion efficiency (PCE) are investigated. The obtained results are contrasted with those of experiments. An optimization process has been done on the configuration increasing the efficiency from 0.49 % to 0.81 %.

Keywords: SCAPS-1D; Dye-sensitized solar cells; Rhamnus tinctoria:soxhlet(emodin dye); Photovoltaic performance; DFT.

1. Introduction

Considering that solar energy is the most abundant renewable energy source on Earth, there is a lot of interest in environmentally friendly methods of turning it into electrical power. To increase efficiency, a variety of methods are now being investigated [1]. As previously said, dye-sensitized solar cells (DSSCs) have seen a notable surge in efficiency in a short time frame, positioning them as one of the more sophisticated technologies because of their promising efficiency. Since the dye-sensitized solar cell was initially introduced by Grätzel et al., there has been a lot of interest in this type of solar cell [1-10]. However, since DSSC efficiency is still below the desired level, more investigation is now necessary. To increase the effectiveness of DSSCs, researchers have worked to enhance the dye, counter electrode, electrolyte, and photoanode [11, 12]. Numerous studies have been released that examine DSSC as a cost-effective and efficient substitute for traditional solar cells [11-14, 15]. DSSCs are made using quick, easy, and affordable methods. One of the fundamental tasks needed to obtain high PCE is the design and manufacturing of photoanodes with enhanced charge transportability, light scattering, and dye loading while concurrently reducing recombination reactions. The majority of the photoanodes are made of metal oxides in the form of mesoporous structures, including TiO_2, ZnO, Nb_2O_5, GaAs, CdS, and SnO_2 [15-17]. Because solar energy is so abundant and exceeds our current global yearly energy needs by a factor of 10,000, photovoltaics is a crucial field among renewable energy sources. For scientists, politicians, and the global economy as a whole, harnessing the vast potential of free energy is an intriguing challenge.

The photovoltaic industry is currently dominated by conventional inorganic semiconductor technology, Such as silicon-based and thin-film solar cells. Significant price reductions and an impressive rise in energy conversion efficiencies were the results of drastic advancements in device manufacturing. However, these devices will always require the use of exceptionally pure starting materials and relatively complex production techniques due to several basic notions of traditional inorganic pn-junction solar cells [18]. One of the most potential green energy sources for creating a low-carbon economy is solar energy, which provides 99 % of the energy on Earth. One effective way to address today's energy issues is to directly convert solar energy into electrical power. Dye-sensitized solar cells (DSSCs) are a type of riverside photovoltaic technology that have attracted significant interest due to its low cost and exceptional energy conversion capabilities. A typical DSSC is composed of an electrolyte with redox couplings dissolved in an organic solvent, sandwiched between a counter electrode (CE) and an organic dye-sensitized TiO_2 anode. In addition to optimizing materials for liquid electrolyte DSSC operation, researchers are recently concentrating on comprehending and enhancing charge generation, recombination, transport, and collection [19]. Compared to traditional solar cells, dye-sensitized solar cells (DSSCs) provide several advantages, including low cost and non-toxicity, ease of manufacture, and the possibility of integrating them into smart.

Numerous outstanding investigations on the manufacturing of inexpensive, highly effective solar cells have been conducted [12]. On the surface of the oxide layer, dye molecules readily absorb sunlight or artificial light and excite electrons by accumulating the incoming photon flux. Excited electrons are injected into the conduction band, increasing its electron population but not filling it completely. The metal

oxide thin layer carries these electrons to the current collector, while an electron donor renews the dye molecule in the redox solution. A complete regeneration is eventually accomplished by transferring electrons to the electron acceptor on the cell's counter electrode [12]. **Figure 1** illustrates how a typical DSSC operates.

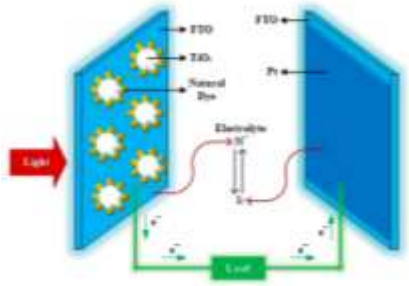

Fig. 1 Principle of operation of a typical DSSC [11]

Natural plant-based organic dyes are widely used in a variety of industries, including medicines, antiviral medication research, and the textile sector [12]. The fruits of Rubia fruticosa, the seeds of Rhamnus tinctoria, and the bark of Pinus pinea are also utilized as dyestuffs. TiO_2 is combined with Rhamnus tinctoria. TiO_2 is the most commonly utilized semiconductor metal oxide in DSSCs because of its many advantages, including its abundance, environmental friendliness, and ability to provide the surface area required for optimal dye loading [12, 21-24]. TiO_2's capacity to absorb a significant amount of incoming light is the primary reason that promotes its adoption in DSSCs [12]. In DSSCs, TiO_2 is often in the anatase or rutile phase. Because of its broadband gap and chemical stability, anatase TiO_2 is utilized more frequently [12]. In this study, dye-sensitized solar cells were modeled and simulated. A useful method for the theoretical investigation of these cells is numerical simulation [24]. Numerical simulation results can shed light on the internal physics and functioning of solar cells. There have been reports of solar cell numerical simulations utilizing program SCAPS-1D program. Numerous factors, including the impact of temperature, interface state density, ETL, active layer and HTL thickness, and ETL electron affinity, has been examined in this study. V_{OC}, $J_{SC,}$ FF, and PCE have all been evaluated in this paper. Theoretical simulation results were compared with published experimental data, showing a high degree of agreement [12]. The numerical simulation structure has been optimized in this paper.

2. Modelling-Simulation of a DSSC Structure

To gain a critical understanding of the concepts underlying photovoltaic (PV) technology, computational modeling techniques have been utilized [13]. Clarifying the mechanical, optical, and electrical characteristics as well as how these microscopic factors impact intricate solar cell systems is crucial. In this study, SCAPS-1D (version 3.3.07) is used for computational modeling and one-dimensional microscopic simulations [1, 5, 12,13, 24]. The SCAPS-1D has been used to study the current-voltage characteristics of solid state dye sensitized solar cells ($ssDSSC_s$) at 1000 Wm^{-2} under the air mass (AM 1.5G) [14]. SCAPS-1D provides recombination models, including Shockley–Read–Hall, Auger recombination, and radiative recombination [15]. This model consisted of five layers FTO/TiO_2/ Rhamnus tinctoria dye/ liquid electrolyte/Pt. The series resistance (Rs) is equal to $100\Omega.cm^2$ in this type. Depending on certain input settings, the new window in SCAPS enables the creation of solar cell layers. The exact measurements that must be made after the solar cell is constructed are as follows: quantum efficiency, current-voltage, and capacitance–frequency. The code computes the designated measurements when the "single-shot" is clicked [15, 16]. Experimental data was used to determine some of the study's input parameters. The density functional theory (DFT) computations were used to analyze the electronic characteristics as shown in **Figure 2** [11, 17]. To determine the relationship between the manufactured surfactants' molecular structures and their abrasion-protective properties, DFT investigations were conducted [17]. Nowadays, a lot of researchers employ density function al theory as a crucial and significant instrument to comp rehend the chemical characteristics of molecules and m aterials. In order to maximize the performance of the suggested cell architecture, accurate estimations on ETL and HTL thicknesses, change in temperature, ETL affinity, and defect density at interface between ETL/active layers.

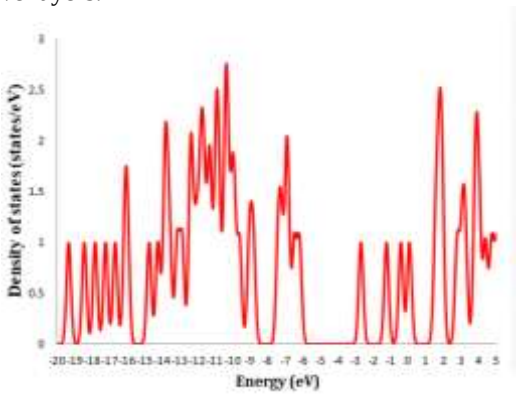

Fig. 1 Density of States by Using DFT Theory

Table 1

The important simulation parameters that were used in this simulation

Material properties	FTO	TiO_2	Rhamnus	Liquid	Reference

			tinctoria dye	electrolyte	
Thickness W (µm)	0.06	15	0.04	25	[11]
Bandgap E_g (eV)	3.7	3.2	1.74	2.7	[11, 15]
Electron affinity χ (eV)	4.4	4.3	3.7	2.5	[11, 15, 21]
Dielectric permittivity ε_r	9	10	4	9	[11, 19, 22]
Effective density of states for CB N_c (cm^{-3})	2.2×10^{18}	1×10^{19}	2.24×10^{18}	1×10^{19}	[11, 18]
Effective density of states for VB N_v (cm^{-3})	1.8×10^{19}	1×10^{19}	2.24×10^{18}	1×10^{19}	[7, 11]
Electron mobility μ_n (cm^2/Vs)	3×10^{1}	1×10^{2}	1×10^{-6}	2×10^{1}	[11, 13]
Hole mobility μ_p (cm^2/Vs)	5×10^{0}	3×10^{1}	5.3×10^{-1}	5×10^{0}	[11]
Shallow uniform donor density N_D (cm^{-3})	10^{20}	1×10^{15}	10^{16}	0	[11]
Shallow uniform acceptor density N_A (cm^{-3})	0	0	10^{16}	$1x10^{18}$	[11]
Defect density N_t (cm^{-3})	1×10^{14}	2×10^{13}	4×10^{5}	1×10^{13}	[11]

The architecture is FTO/TiO_2/ Rhamnus tinctoria dye /liquid electrolyte/pt. The cell's structural assembly is displayed in **Figure 3a**. After illumination, the electron-hole pairs are produced in the Rhamnus tinctoria dye. Excitons dissolve at the i–p interface, causing holes to migrate to the HTL layer and the remaining electrons to diffuse to the ETL layer. The movement mechanism of excitons is summarized in **Figure 3b**. The effect of the ETL, active layer, and HTL thicknesses, working temperature, electron affinity of ETL, and defect density at the interface between the active layer and ETL on different parameters of the DSSC are studied. In each case, V_{OC}, FF, J_{SC}, and PCE parameters are analyzed. An optimization process has been done on the structure increasing the efficiency from 0.49 % up to 0.811%.

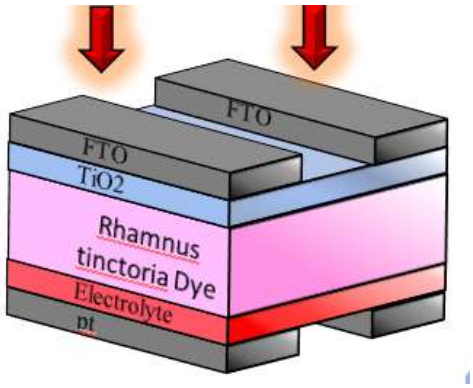

(a)

Fig. 2 (a) Device archeticture of the dye sensitized solar cell and (b) HOMO-LUMO band diagram

After obtaining a J-V curve that is as similar to the empirically observed J-V curve as possible, the calibrated input SCAPS 1-D simulation parameters are recorded (see **Table 2**) as shown in **Figures 4** [11]**.**

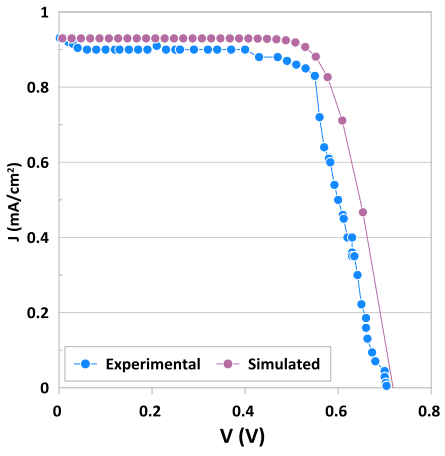

Fig. 3 Calibration J-V Curve for a DSSC.

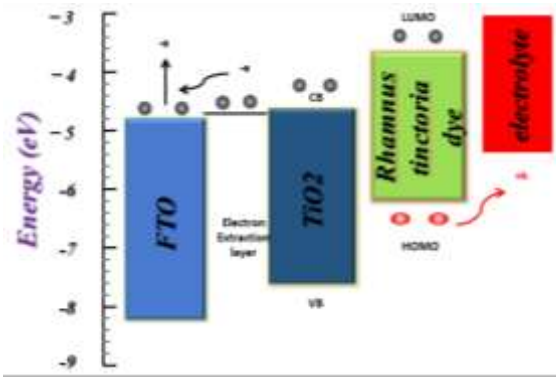

(b)

Table 1 PV calibration compared with experimental and simulated results.

	J_{SC} (mA/cm^2)	V_{OC} (V)	FF (%)	PCE (%)
Experimental	0.92	0.71	72	0.47
Simulated	0.93	0.72	72.7	0.49

There is a strong correlation between the measurements and our model, demonstrating that our simulation is accurate. Analyses are conducted in the next section to examine how the device's primary components affect cell performance. These analyses include changing absorber layer, ETL, and HTL thicknesses and defect density at the dye/TiO_2 interface. Also, the working temperature and the affinity of ETM are investigated. Every parameter is optimized to obtain the highest PCE achievable.

3. Results and Discussion

3.1 Impact of Altering the Thicknesses of ETL and HTL

Our simulation covers the effect of changing HTL/ETL thicknesses in the ranges of (5 µm–35 µm) and (5 µm–50 µm) for ETL and HTL, respectively as illustrated in **Fig. 5**.

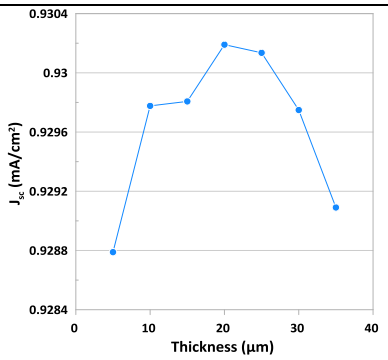

(a)

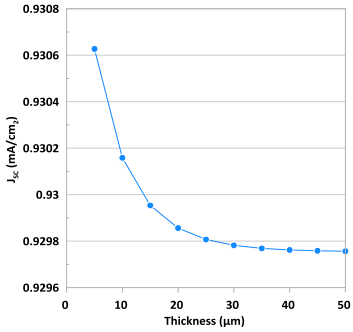

(b)

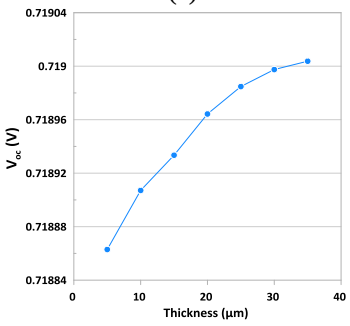

(c)

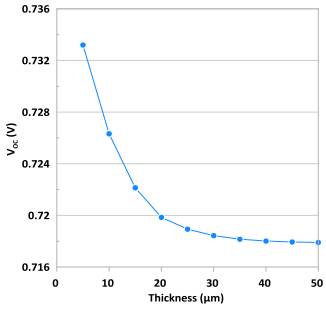

(d)

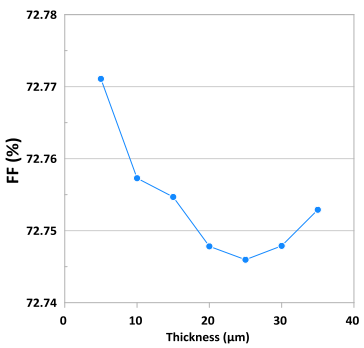

(e)

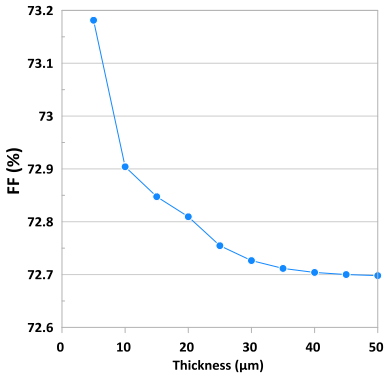

(f)

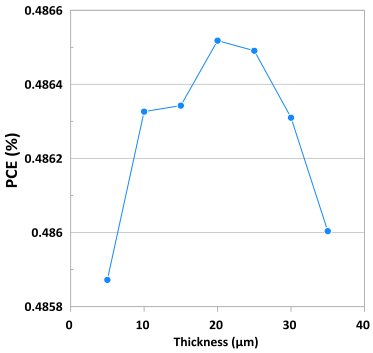

(g)

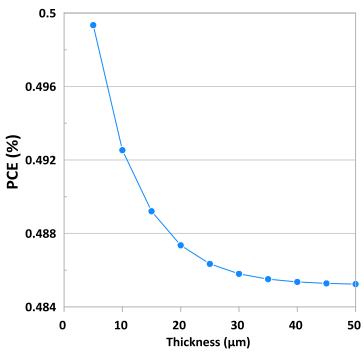

(h)

Fig. 4. Effect of thickness of (left-hand side) ETL and (right-hand side) HTL on the cell parameters.

As seen from **Figure 5**, the J_{SC} increases from 0.92878 to 0.93019 mA/cm^2 when the thickness of TiO_2 increases from 5 to 20 µm and then decreases when the TiO_2 thickness increases above 20 up to 35 µm. The DSSC efficiency and TiO_2 film thickness exhibit a similar trend, displaying the highest possible efficiency value of 0.486518 % for the 20 µm of TiO_2 film. These findings imply that the short-circuit photocurrent density primarily determines the efficiency of these DSSCs [23]. The improvement of efficiency when the TiO_2 thickness increased from 5 to 20 µm is shown in **Figure 5**. The rise in injection electrons from LUMO of excited dyes to the conduction band of TiO_2 is connected to the increase in Jsc up to this specific thickness [23]. Despite having a greater total surface area within the nanoporous structure, nanocrystalline TiO_2 films thicker than the above-optimized thickness most likely result in a higher electron transport series resistance, which in turn enhances electron recombination with I3-ions at the TiO_2 surface, lowering the Jsc value and efficiency [23]. As thickness increases, recombination in the electron transfer mechanism in TiO_2 nanoparticles would cause more injected electrons to be lost, raising the DSSC's R_2CT and decreasing efficiency [23]. Conversely, light has a harder time efficiently reaching the TiO_2/dye/electrolyte junction when the TiO_2 coating is thicker. Consequently, thicker TiO_2 electrodes result in lower efficiency and J_{sc} values [23]. From the data obtained, the voltage is directly proportional to the thickness of TiO_2 and this is consistent with what Zulkifli Amin *et al* found [5]. The FF decreases as the thickness increases because the series resistance rises with thickness up to 25µm and then increases, this is consistent with what Najwa Chawki *et al* found [24]. To optimize PCE and photo-thermal stabilities, the HTL is essential to the cell's overall performance [15]. The effect of HTL thickness on the behavior of DSSC is demonstrated in Fig. 5. "right hand side". The thickness of HTL was altered within the range of 5–50 µm and its effect on the V_{OC}, J_{SC}, FF, and PCE of the DSSC is investigated. We can obtain the cell's ideal HTL thickness in this way. Due to an increase in series resistance, the thickness causes a minor decrease in the V_{OC}, FF, PCE, and J_{SC} [14, 25, 26], this is consistent with what S. Abdelaziz *et al* found [13]. Efficiency reaches a maximum value of 0.499 % at 5 µm for HTL.

3.2 Effect of Changing Absorber Layer Thicknesses:

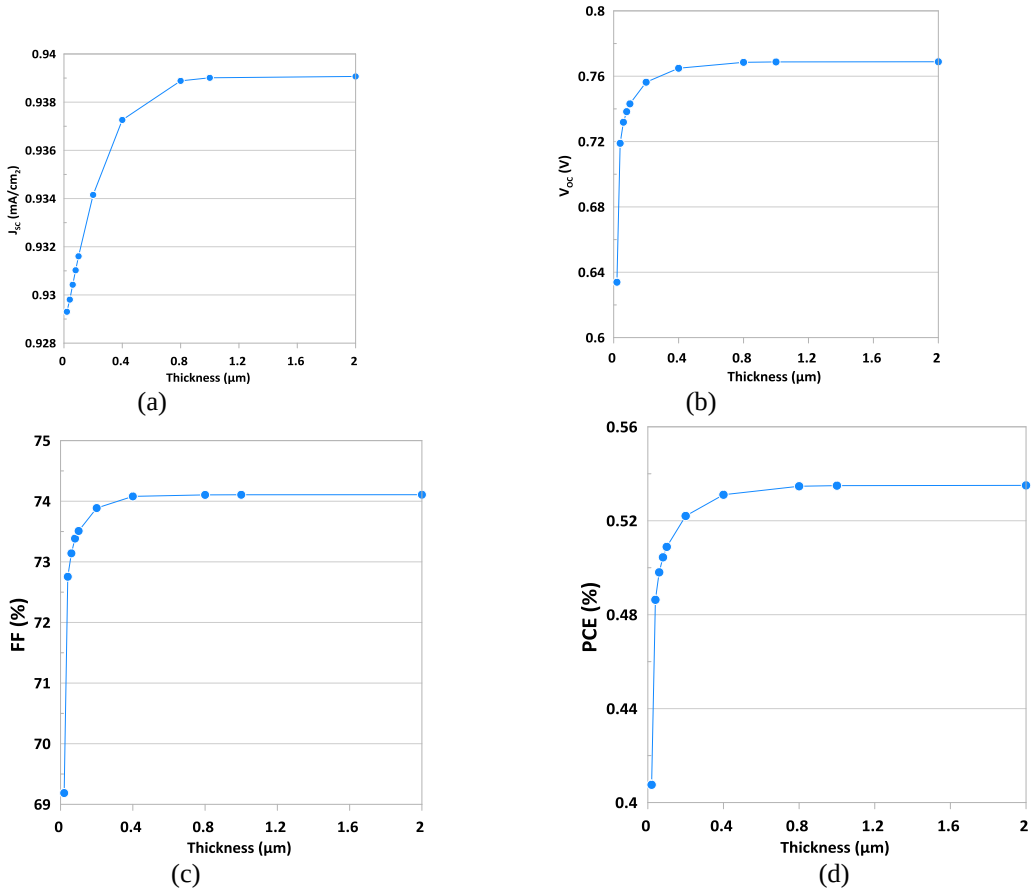

Figure 5 Effect of thickness of active layer on the cell parameters.

Fig. 6 illustrates the dependence of the J_{SC}, V_{OC}, FF, and PCE according to the changing of the active-layer thickness. The thickness of the active layer Rhamnus tinctoria dye was varied from 0.02 µm to 10 µm using the SCAPS-1D computational code. Photons that are transformed into electricity at the cell's p-i-n junction are absorbed by the dye [15]. Solar radiation should be absorbed by the pigments used in PV technology in the visible and near-infrared (IR) spectrum (300–900 nm) [15]. More absorption and higher cell characteristics are achieved by increasing the absorber thickness by the same amount as the diffusion length [13]. Since they are directly related to one another, we were able to increase the J_{SC}, V_{OC}, and FF to raise the efficiency (ɳ %) and, consequently, the rate of energy absorption. The number of carriers produced increased as the absorption layer's thickness increased [15, 21]. At 10 µm, the J_{SC} extent a maximum value of 0.939 mA/cm^2 whereas the efficiency increases and attains a maximum of 0.535 %.

3.3 Effect of Temperature

The ambient temperature in a given environment has a major effect on the performance of DSSCs [15]. Since solar cell devices are typically placed outside, their thermal stabilities deteriorate over time as a result of exposure to high temperatures, particularly in the summer [15]. Solar cells often function at temperatures higher than 300 K. Additionally, current third-generation solar cells may be mounted on windows and are also effective in diffuse environments. As a result, research into how temperature changes affect cell performance is required. In this research, the temperature was varied from 280 to 400 K. The output in **Figure 7a, 7b** shows that both J_{SC} increased while V_{OC} decreased as the temperature was raised from 280 to 400 K. As presented in **Figure 7c and 7d** the PCE and FF decreased when the temperature changed from 280 to 400 K. The usable lives of semiconductors decrease as the temperature rises. Interestingly, PV devices deteriorate and the performance drop in terms of efficiency at high temperatures because they are unstable [15]. The formula for a solar cell device's efficiency is given by **Eq 1**,

$$\text{PCE} = \frac{Pmax}{Pin} = \frac{VOC \times JSC \times FF}{Pin} \times 100\ \% \quad \textbf{(1)}$$

Eq 2 gives the relationship of V_{OC}, FF, and J_{SC};

$$FF = \frac{Pmax}{VOC \times JSC} = \frac{Jmp \times Vmp}{VOC \times JSC} \quad \textbf{(2)}$$

As the temperature is raised from 280 to 400 K, there is an increase in J_{SC} from 0.92978 to 0.92987 mA/cm^2. When the thermal activation energy rises due to a temperature increase, this rise is linked to a decrease in the charge recombination. Additionally, it is mentioned that the V_{OC} decreases from 0.75507 to 0.53485 V when the temperature increases from 280 to 400 K. A rise in the dark saturation current J0 and, eventually, large rates of carrier charge recombination are blamed for this decline. The Voc depends on JSC, as predicted by **Eq 3**;

$$VOC = \frac{nKB\,T}{q} \ln\left[\frac{JSC}{J0} + 1\right] \quad \textbf{(3)}$$

As T is the absolute temperature in (K), K_B is the Boltzmann constant (K_B = 1.38 × 10^{-23} J/K), q is the electron charge (q = 1.603 × 10^{-19} C), n is the ideality factor, and J_{SC} is the generated current in the presence of light illumination. The thermal voltage is denoted by the notation nK_BT/q [15, 22].

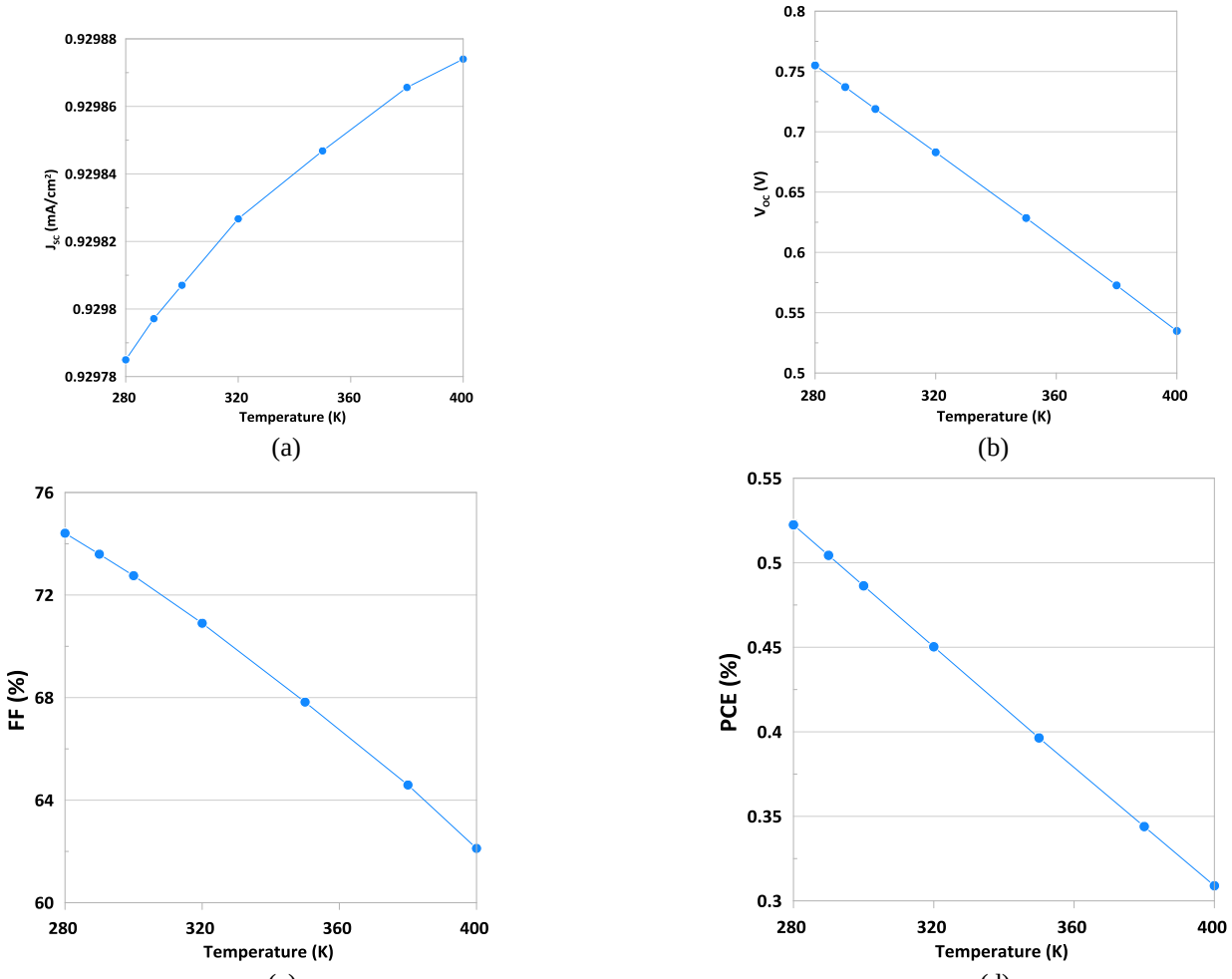

Fig. 6 : Effect of working temperature on the cell parameters.

3.4 Effect of the Conduction Band of TiO_2:

The electron affinity has been changed from 4 eV to 4.5 eV for ETL as shown in **Figure 8**. The optimum value for ETL is 4.1 eV, achieving an efficiency of 0.6386 %. As appears in **Figure 8**, the ideal affinities result in a smaller band gap offset between the active layer's HOMO level and the valence band of the HTL and between the photoactive layer's LUMO level and the conduction band of the ETL. Because of this alignment, there is less energy loss, it increases the built-in voltage and electric field and makes it easier for charge carriers to be efficiently extracted from the active layer and transferred to the carrying layers [26].

3.5 Effect of Defect at the Interface Between TiO_2 and Active Layer:

Defect density at ETL/acive layer interface was changed from 10^8 cm^{-2} to 10^{14} cm^{-2}. Defects change Jsc from 0.9298 mA/cm^2 to 0.92941 mA/cm^2 which causes to a change in the efficiency from 0.650429 % to 0.34226 % as shown in **Table 3**. Because light enters via TiO_2 and the majority of carrier production takes place around this interface, defect density at ETL has a significant impact on J_{SC} [27].

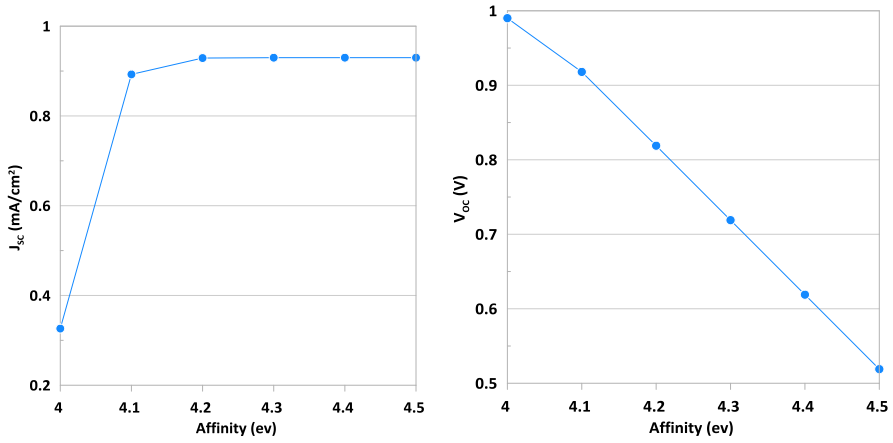

(a) (b)

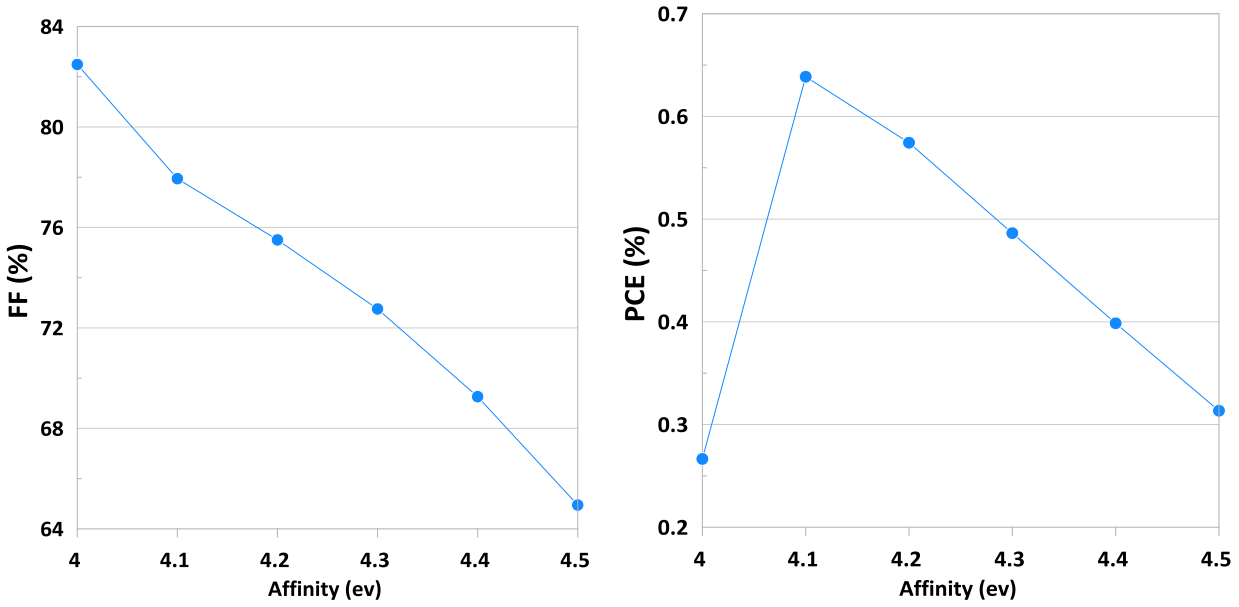

(b) (d)

Fig. 7: Effect of electron affinity of TiO_2 on the cell parameters.

Table 3 The DSSCs cell performance characteristics for the different defects at the interface between TiO_2 and active layer

Defect at interface	Jsc (mA/cm2)	Voc (V)	FF (%)	eta (%)
1.00E+08	9.30E-01	9.10E-01	7.69E+01	6.50E-01
1.00E+09	9.30E-01	8.44E-01	7.59E+01	5.95E-01
1.00E+10	9.30E-01	7.80E-01	7.45E+01	5.40E-01
1.00E+11	9.30E-01	7.19E-01	7.28E+01	4.86E-01
1.00E+12	9.30E-01	6.58E-01	7.08E+01	4.33E-01
1.00E+13	9.30E-01	5.99E-01	6.85E+01	3.82E-01
1.00E+14	9.29E-01	5.55E-01	6.63E+01	3.42E-01

4. Optimization of Effects for Dye-Sensitized Solar Cell:

To conduct the study that illustrates their impact on the PV characteristics of the dye solar cell, the thicknesses of the ETL, HTL, and active layer are altered. Additionally examined are the ETL layer's affinity, interface defect density, and operating temperature, all of which have an impact on the device's performance. After a careful analysis of all the effects, the structure underwent optimization, resulting in an increase in efficiency from 0.49 % to 0.81 %, as shown in **Figure 9.**

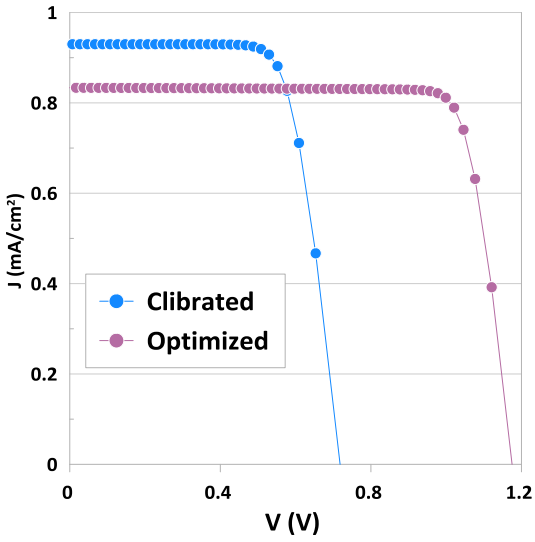

Fig. 8: the optimized DSSC.

5. Conclusion

The SCAPS 1D software and DFT theory have been used to simulate and calibrate a dye-sensitized solar cell. The effect of ETL, HTL, and active layer thicknesses, working temperature, the affinity of ETL, and the interface between TiO_2 and active layer on different parameters of the DSSC are studied. Reasonable modifications were made to maximize the overall performance of the cell on ETL and HTL thicknesses, working temperature, Rhamnus tinctoria dye thickness, the affinity of TiO_2, and the interface between TiO_2 and active layer on different parameters. The highest optimized performance values: are J_{sc} of 0.833 mA/cm^2, PCE of 0.811 %, V_{oc} =1.18 V, and FF =82.65%.

References

[1] M. E. Yeoh, K. Y. Chan, and H. Y. Wong, "Investigation on the thickness effect of tio2 photo-anode on dye-sensitized solar cell performance," *Solid State Phenom.*, vol. 280 SSP, pp. 76–80, 2018, doi: 10.4028/www.scientific.net/SSP.280.76.

[2] A. Gunasekaran, H. Ying, V. K. Ponnusamy, and A. Sorrentino, "Synthesis of high polydispersity index polylactic acid and its application as gel electrolyte towards fabrication of dye‐sensitized solar cells," *J. Polym. Res.*, 2021, doi: 10.1007/s10965-021-02615-w.

[3] L. Zhang, G. Boschloo, L. Hammarström, and H. Tian, "Solid state p-type dye-sensitized solar cells: Concept, experiment and mechanism," *Phys. Chem. Chem. Phys.*, vol. 18, no. 7, pp. 5080–5085, 2016, doi: 10.1039/c5cp05247e.

[4] F. Jahantigh and M. Javad, "The effect of HTM on the performance of solid‐state dye‐sanitized solar cells (SDSSCs): a SCAPS‐1D simulation study," *Appl. Phys. A*, pp. 1–7, 2019, doi: 10.1007/s00339-019-2582-0.

[5] Z. Amin, I. Ridwan, and M. F. Aziz, "Effect of Titanium Dioxide Thickness on Performance of DSSC Solar Cell Using Red Dragon Fruit Dye," *J. Adv. Res. Fluid Mech. Therm. Sci.*, vol. 96, no. 2, pp. 172–181, 2022, doi: 10.37934/arfmts.96.2.172181.

[6] S. A. Elroby and A. Jedidi, "Density functional theory study on two D-π-A-type organic dyes containing different anchoring groups for dye-sensitized solar cells," *Struct. Chem.*, vol. 31, no. 3, pp. 1125–1135, 2020, doi: 10.1007/s11224-020-01489-w.

[7] M. Bavarian, S. Nejati, K. K. S. Lau, D. Lee, and M. Soroush, "Theoretical and experimental study of a dye-sensitized solar cell," *Ind. Eng. Chem. Res.*, vol. 53, no. 13, pp. 5234–5247, 2014, doi: 10.1021/ie4016914.

[8] H. J. Snaith and L. Schmidt-Mende, "Advances in liquid-electrolyte and solid-state dye-sensitized solar cells," *Adv. Mater.*, vol. 19, no. 20, pp. 3187–3200, 2007, doi: 10.1002/adma.200602903.

[9] M. Sutton, B. Lei, H. Michaels, M. Freitag, and N. Robertson, "Rapid and Facile Fabrication of Polyiodide Solid-State Dye-Sensitized Solar Cells Using Ambient Air Drying," *ACS Appl. Mater. Interfaces*, vol. 14, no. 38, pp. 43456–43462, 2022, doi: 10.1021/acsami.2c14299.

[10] S. Shalini, R. Balasundaraprabhu, T. Satish Kumar, N. Prabavathy, S. Senthilarasu, and S. Prasanna, "Status and outlook of sensitizers/dyes used in dye sensitized solar cells (DSSC): a review," *Int. J. Energy Res.*, vol. 40, no. 10, pp. 1303–1320, 2016, doi: 10.1002/er.3538.

[11] F. Aslan, "New natural dyes extracted by ultrasonic and soxhlet method: Effect on dye-sensitized solar cell photovoltaic performance," *Opt. Quantum Electron.*, vol. 56, no. 4, pp. 1–22, 2024, doi: 10.1007/s11082-024-06294-x.

[12] D. Kumar, P. Kuchhal, and K. S. Parmar, "Optimization of photovoltaic conversion performance of a TiO2 based dye sensitized solar cells (DSSCs)," *Eng. Res. Express*, vol. 3, no. 4, 2021, doi: 10.1088/2631-8695/ac372e.

[13] S. Abdelaziz, A. Zekry, A. Shaker, and M. Abouelatta, "Investigating the performance of formamidinium tin-based perovskite solar cell by SCAPS device simulation," *Opt. Mater. (Amst).*, vol. 101, no. February, pp. 3–10, 2020, doi: 10.1016/j.optmat.2020.109738.

[14] A. N. M. Alahmadi, "Design of an Efficient PTB7 : PC70BM-Based Polymer Solar Cell for 8 % Efficiency," 2022.

[15] B. K. Korir, J. K. Kibet, and S. M. Ngari, "Simulated performance of a novel solid-state dye-sensitized solar cell based on phenyl-C61-butyric acid methyl ester (PC61BM) electron transport layer," *Opt. Quantum Electron.*, vol. 53, no. 7, pp. 1–24, 2021, doi: 10.1007/s11082-021-03013-8.

[16] G. A. Nowsherwan *et al.*, "Performance Analysis and Optimization of a PBDB-T : ITIC Based Organic Solar Cell Using Graphene Oxide as the Hole Transport Layer," 2022.

[17] M. M. Khalaf *et al.*, "Journal Pre-proof," 2019.

[18] K. A. Ojotu and G. Babaji, "Simulation of an Optimized Poly 3-Hexylthiophene (P3HT) based solid state Dye Sensitized Solar Cell (ss-DSSC) using SCAPS," vol. 5, no. 2, pp. 1–10, 2020.

[19] T. Delgado-Montiel, R. Soto-Rojo, J. Baldenebro-López, and D. Glossman-Mitnik, "Theoretical study of the effect of different π bridges including an azomethine group in triphenylamine-based dye for dye-sensitized solar

cells," *Molecules*, vol. 24, no. 21, pp. 1–16, 2019, doi: 10.3390/molecules24213897.

[20] N. Rono, A. E. Merad, J. K. Kibet, B. S. Martincigh, and V. O. Nyamori, "A theoretical investigation of the effect of the hole and electron transport materials on the performance of a lead-free perovskite solar cell based on CH3NH3SnI3," *J. Comput. Electron.*, vol. 20, no. 2, pp. 993–1005, 2021, doi: 10.1007/s10825-021-01673-z.

[21] R. K. Z. , Et. al., "Effect Of Carrier Concentration And Thickness Of Absorber Layer On Performance CBTS Solar Cell," *Turkish J. Comput. Math. Educ.*, vol. 12, no. 10, pp. 5056–5064, 2021, doi: 10.17762/turcomat.v12i10.5281.

[22] P. Sawicka-Chudy *et al.*, "Simulation of TiO2/CuO solar cells with SCAPS-1D software," *Mater. Res. Express*, vol. 6, no. 8, 2019, doi: 10.1088/2053-1591/ab22aa.

[23] L. Dissanayake and C. A. Thotawatthage, "The effect of TiO2 photo anode film thickness on photovoltaic properties of dye-sensitized solar cells The effect of TiO 2 photoanode film thickness on photovoltaic properties of dye-sensitized solar cells," no. October, 2016, doi: 10.4038/cjs.v45i1.7362.

[24] N. Chawki, "Numerical Study of BaZrS 3 Based Chalcogenide Perovskite Solar Cell Using SCAPS-1D Device Simulation," pp. 1–18, 2022.

[25] N. Rai, S. Rai, P. Kumar, S. Pooja, and L. D. K. Dwivedi, "Analysis of various ETL materials for an efficient perovskite solar cell by numerical simulation," *J. Mater. Sci. Mater. Electron.*, vol. 1, no. 0123456789, 2020, doi: 10.1007/s10854-020-04175-z.

[26] W. Abdelaziz, A. Shaker, M. Abouelatta, and A. Zekry, "Possible efficiency boosting of non-fullerene acceptor solar cell using device simulation," *Opt. Mater. (Amst).*, vol. 91, no. March, pp. 239–245, 2019, doi: 10.1016/j.optmat.2019.03.023.

[27] A. S. Chouhan, N. P. Jasti, and S. Avasthi, "Effect of Interface Defect Density on Performance of Perovskite Solar Cell : Correlation of Simulation and Experiment," vol. 1, 2018.